Environmental Science and Pollution Research (2023) 30:71543–71553
https://doi.org/10.1007/s11356-021-13597-z

CIRCULAR ECONOMY FOR GLOBAL WATER SECURITY

High-efficient reduction of methylene blue and 4-nitrophenol by silver nanoparticles embedded in magnetic graphene oxide

Van-Dat Doan[1] · Ngoc-Vy Nguyen[1] · Thi Lan-Huong Nguyen[2] · Vy Anh Tran[3] · Van Thuan Le[4,5]

Received: 3 January 2021 / Accepted: 17 March 2021 / Published online: 26 March 2021

Abstract

In this study, a ternary magnetically separable nanocomposite of silver nanoparticles (AgNPs) embedded in magnetic graphene oxide (Ag/Fe_3O_4@GO) was designed and synthesized. Beta-cyclodextrin was used as a green reducing and capping agent for decorating of AgNPs on Fe_3O_4@GO. The fabricated material was characterized using X-ray diffractometry, Fourier transform infrared spectroscopy, scanning electron microscopy, vibrating sample magnetometry, and energy-dispersive X-ray spectroscopy. The catalytic properties of the prepared Ag/Fe_3O_4@GO for the reduction of 4-nitrophenol (4-NP) and methylene blue (MB) dye with sodium borohydride were investigated in detail. The morphological and structural studies revealed that Fe_3O_4 and AgNPs with a mean size of 12 nm were uniformly distributed on the GO sheet at high densities. The catalytic tests showed that Ag/Fe_3O_4@GO exhibited an ultrafast catalytic reduction of 4-NP and MB with a reduction rate constant of 0.304 min^{-1} and 0.448 min^{-1}, respectively. Moreover, the catalyst demonstrated excellent stability and reusability, as evidenced by the more than 97% removal efficiency maintained after five reuse cycles. The Ag/Fe_3O_4@GO catalyst could be easily recovered by the magnetic separation due to the superparamagnetic nature of Fe_3O_4 with high saturated magnetization (45.7 emu/g). Besides, the formation of networking between the formed AgNPs and β-CD through hydrogen bonding prevented the agglomeration of AgNPs, ensuring their high catalytic ability. The leaching study showed that the dissolution of Fe and Ag from Ag/Fe_3O_4@GO was negligible, indicating the environmental friendliness of the synthesized catalyst. Finally, the high catalytic performance, excellent stability, and recoverability of Ag/Fe_3O_4@GO make it a potential candidate for the reduction of organic pollutants in wastewater.

Keywords Graphene oxide · Magnetic nanocatalyst · Silver nanoparticles · Methylene blue · 4-Nitrophenol · Reduction

Introduction

Water pollution by organic compounds discharged from textile, printing, and pharmaceutical factories has caused many serious environmental problems. Due to their non-biodegradable nature and high toxicity, most of the organic pollutants may have negative effects on human and animal health, including mutations and cancer (Lim et al. 2020; Luu et al. 2020; Tran et al. 2020d). For example, the existence of methylene blue (MB), one of the most commonly used organic dyes, in wastewater can interfere with the photosynthesis and oxygen exchange of aquatic organisms (Dao et al. 2020; Tran et al. 2020c). Another hazardous organic refractory substance usually found in industrial and agriculture effluents due to its high solubility and long-term stability in water is 4-nitrophenol (4-NP) (Ismail et al. 2019). It has been reported to be toxic to aquatic life and cause several human health problems such as damaging the liver, kidneys, blood, and central nervous system (Liu et al. 2018). Because of these

Responsible Editor: Santiago V. Luis

✉ Vy Anh Tran
tranhvy@gmail.com

✉ Van Thuan Le
levanthuan3@duytan.edu.vn

[1] Faculty of Chemical Engineering, Industrial University of Ho Chi Minh City, 12 Nguyen Van Bao, Ho Chi Minh 700000, Vietnam

[2] Institute of Biotechnology and Food Technology, Industrial University of Ho Chi Minh City, Ho Chi Minh 700000, Vietnam

[3] Department of Chemical and Biological Engineering, Gachon University, 1342 Seongnamdaero, Sujeong-gu, Seongnam-si 13120, Republic of Korea

[4] Center for Advanced Chemistry, Institute of Research and Development, Duy Tan University, Da Nang 550000, Vietnam

[5] The Faculty of Environmental and Chemical Engineering, Duy Tan University, Da Nang 550000, Vietnam

issues, finding effective methods for treating organic pollutants from wastewater has received much attention from many scientists over the past decade.

Recently, the reduction with sodium borohydride ($NaBH_4$) is considered one of the most promising way for removing aromatic dyes and nitrocompounds because of its high efficiency and simplicity in implementation (Xu et al. 2020). However, the reduction is only favourable in the presence of catalysts, which are usually noble metal nanoparticles (NPs) (e.g., Ag. Au, Pt) owing to their unique photoelectric properties (Doan et al. 2020). Among these metal NPs, AgNPs are extensively used because they possess outstanding properties such as low-cost, easy synthesis, large surface to volume ration, different crystallographic facets, and excellent catalytic activity (Kavyani and Baharfar 2020; Nguyen et al. 2020). Nevertheless, ultrafine AgNPs with high surface energy tend to agglomerate in clusters, reducing their catalytic performance. Besides, the difficulty in recovering the nano-sized catalysts after use also limits their reusability and practical application. At present, the utilization of support materials such as polymer matrices, metal-organic frameworks, and carbon-based materials for immobilizing NPs has been reported as the most effective approach to overcome the above disadvantages (Le et al. 2020; Tran et al. 2021). The catalyst supports can hinder the aggregation, facilitate the recovery, and improve the stability and catalytic efficiency of NPs. As an emerging class of carbon-based materials, graphene oxide (GO) has shown excellent potential as a substrate for various catalysts and sensors due to its large surface area, tailorable surface chemistry, high mechanical strength and flexibility, and high chemical and thermal stability (Tran et al. 2020b). For instance, Kumari et al. successfully synthesized GO/AgNP composite using a sonochemical method and applied it for the degradation of MB dye. The study results revealed that the fabricated GO/AgNPs showed a superior catalytic activity compared with the pristine GO and AgNPs (Kumari et al. 2020). Investigating the reduction of 4-NP on polyacrylamide/polypyrrole/GO supported AgNPs, Mao et al. also demonstrated the crucial role of GO in enhancing the catalytic ability of the resultant nanocomposite (Mao et al. 2018). In recent years, GO is often integrated with Fe_3O_4 NPs to increase the recoverability and reusability of catalysts (Esmaeili et al. 2019; Kavyani and Baharfar 2020). With strong magnetic property, the presence of Fe_3O_4 NPs in catalysts makes them easily recovered by an external magnetic field.

In this context, the purpose of this study was to simultaneously combine the catalytic and magnetic functionalities of Ag and Fe_3O_4 NPs into the GO support for the catalytic reduction of MB and 4-NP solutions with $NaBH_4$. This ternary nanocomposite was fabricated by the decoration of AgNPs onto the pre-synthesized Fe_3O_4@GO hybrid using beta-cyclodextrin (β-CD) as a capping agent. β-CD was chosen as a green substance for reducing Ag^+ ions and stabilizing the formed AgNPs on the GO sheets due to its high biocompatibility and environmental friendliness, and its unique conformation. With the large structure and rich hydroxyl groups, β-CD can encapsulate AgNPs to restrict their agglomeration and well immobilize them to the GO surface by hydrogen bonding. The resulting hybrid nanocomposite was comprehensively characterized by various physicochemical technologies before evaluating its catalytic ability for MB and 4-NP. The stability, recoverability, and leaching of the developed catalyst were investigated for long-term use. The catalytic mechanism also discussed in detail.

Materials and methods

Materials

Natural graphite flakes (99% carbon basis, 50 mesh particle size), potassium permanganate ($KMnO_4$, ≥ 99%), iron(III) chloride hexahydrate ($FeCl_3.6H_2O$, ≥ 99%), iron(II) sulfate heptahydrate ($FeSO_4.7H_2O$, ≥ 99%), sodium hydroxide (NaOH, ≥ 98%), hydrochloric acid (HCl, 37%), sodium nitrate ($NaNO_3$, ≥ 99%), sulfuric acid (H_2SO_4, 98%), hydrogen peroxide (H_2O_2, 30%), ethanol (C_2H_5OH, 99%), β-cyclodextrin ($C_{42}H_{70}O_{35}$, ≥ 97%), silver nitrate ($AgNO_3$, ≥ 99%), methylene blue ($C_{16}H_{18}ClN_3S$, ≥ 95%), sodium borohydride ($NaBH_4$, ≥ 98%), and 4-nitrophenol ($O_2NC_6H_4OH$, ≥ 99%) were purchased from Merck Company (Singapore).

Synthesis of Ag/Fe_3O_4@GO catalyst

Preparation of GO

The synthesis of GO was performed based on the Hummers' method (Ma et al. 2019). Briefly, 0.5 g of graphite flakes were mixed with 0.5 g of $NaNO_3$ in a heat-resistant glass flask cooled at 0 °C, followed by adding 23 mL of concentrated H_2SO_4 98%, and the resulting mixture was stirred vigorously for 4 h. Then, 3 g of $KMnO_4$ was added to the mixture under constant stirring for another 2 h. After that, 46 mL of distilled water was dropped to the solution, the reaction temperature of 90–95 °C was adjusted by a water bath. Next, 10 mL of H_2O_2 (30%) was added to the flask, followed by stirring for 1 h. The product was then filtered and washed with distilled water until the pH of the solution reached 7. The obtained GO sample was dried at 60 °C for 24 h in a vacuum oven.

Preparation of Fe_3O_4@GO

The decoration of Fe_3O_4 NPs on the as-prepared GO sheets was performed through the co-precipitation reaction. In the first step, the GO solution (1 mg/mL) was prepared by

dispersing 0.05 g GO into 50 mL of distilled water under ultrasound for 30 min. Next, 0.2332 g $FeCl_3.6H_2O$ and 0.1119 g $FeSO_4.7H_2O$ were added to the GO solution, and the mixture was stirred at 60 °C for 30 min before adding 2M NaOH solution to adjust the pH to 10. After vigorously stirred for another 30 min, the obtained Fe_3O_4@GO was separated by a magnet and washed with distilled water until the filtrate was neutral. Finally, the product was dried at 60 °C in a vacuum oven. For comparison, the pure Fe_3O_4 NPs were prepared by the same procedure without GO.

Embedded AgNPs on Fe_3O_4@GO

A calculated amount (0.05 mg) of the as-synthesized Fe_3O_4@GO was dispersed in distilled water (50 mL) under ultrasound for 30 min to obtain a clear solution (1 mg/mL). Then, 25 mL of 0.1M NaOH and 25 mL of 5 mM $AgNO_3$ were added in 50 mL Fe_3O_4@GO solution at room temperature under stirring. Afterwards, 50 mL of β-CD solution (2 g/L) was added to the mixture, followed by ultrasonic irradiation for 30 min. The resulting composite was collected by a hand-magnet, washed with anhydrous ethanol, and dried at 60 °C for 24 h.

Characterization of catalyst

The structural characteristics, morphology, chemical composition, and magnetic properties of the as-synthesized materials were characterized by X-ray powder diffraction (XRD, Rigaku Ultima IV, Japan), Fourier-transform infrared spectroscopy (FTIR, Bruker Tensor 27, Germany), field emission scanning electron microscopy (FE-SEM, Hitachi S-4800, Japan), transmission electron microscopy (TEM, Hitachi H-7600, Japan), energy-dispersive X-ray spectroscopy (EDX, X-ray Micro Analyzer H-7593, Japan), and vibrating sample magnetometer (VSM, VSM-DMS 880, USA).

Catalytic study

The catalytic activity of the prepared materials was evaluated through the reduction of 4-NP and MB in the presence of $NaBH_4$. For a typical experiment, 50 mL of the organic pollutant (0.05 mM of MB or 0.2 mM of 4-NP) was mixed with 5 mL of 0.1 M $NaBH_4$ in a 100 mL beaker. Next, 10 mg of the catalyst was added to the mixture and vigorously shaken. After a selected time period, 2 mL of the mixture was extracted, the catalyst was separated by a hand-magnet, and the pollutant concentrations were determined by UV-Vis spectrophotometer (Agilent Cary 60, USA) at a maximum absorbance wavelength of 664 nm for MB or 405 nm for 4-NP. The removal efficiency of MB and 4-NP was calculated by Eq. 1.

$$\text{Removal efficiency}(\%) = \frac{C_0 - C_t}{C_0}.100\% = \frac{A_0 - A_t}{A_0}.100\% \quad (1)$$

where C_0 and C_t (mg/L) are the concentration of 4-NP/MB at time $t = 0$ and $t = t$, respectively, and A_0 and A_t are the absorbance of 4-NP/MB at the beginning and at any time t, respectively.

Results and discussion

Formation of Ag/Fe_3O_4@GO

The formation of Ag/Fe_3O_4@GO composite can be divided into three steps, as illustrated in Scheme 1. In the first step, GO was obtained by oxidation of natural graphite using the Hummer's method. The presence of oxygen-containing functional groups (-COOH, -OH, ketone, and epoxy) on the GO surface make it well dispersed in water by the hydrogen bonding (Liu et al. 2015). In the next step, Fe^{3+} and Fe^{2+} ions with a molar ratio of 2:1 were dispersed in the GO suspension. The introduced iron ions were then rapidly adsorbed onto the negatively charged surface of GO through electrostatic attraction. Fe_3O_4 particles were in situ formed on GO when NaOH was added to the mixture according to the reaction Eq. 2. (Yazdani and Seddigh 2016). Finally, the Ag/Fe_3O_4@GO composite was obtained by the decoration of AgNPs onto the Fe_3O_4@GO surface using β-CD as a reducing and capping agent. In this step, Ag^+ cations were attracted to the Fe_3O_4@GO surface via electrostatic interaction, and then reduced to AgNPs by β-CD. Due to its special structure consisted of two hydroxyl rings forming a truncated cone, β-CD exhibited high level in controlling the morphology of AgNPs by limiting their shape and size within the boundaries of the hydroxyl rings (Nariya et al. 2020). Furthermore, the formation of networking between the formed AgNPs and β-CD through hydrogen bonding prevented the agglomeration of AgNPs, maintaining their high catalytic ability.

$$Fe^{2+} + 2Fe^{3+} + 8OH^- \rightarrow Fe_3O_4 + H_2O \quad (2)$$

Characterization of catalysts

The structure of the as-synthesized materials was characterized by XRD as shown in Fig. 1a. The XRD pattern of GO showed two characteristic peaks at 2θ of 10.5° and 42.6° (Le et al. 2019). The diffraction peaks at 2θ of 30.1°, 35.2°, 41.4°, 45.5°, 56.4°, and 62.5° ascribed to the (220), (311), (400), (422), (511), and (440) lattice planes of the cubic spinel crystal structure of Fe_3O_4 were detected in the XRD patterns of both Fe_3O_4/GO and Ag/Fe_3O_4@GO. According to the XRD spectrum of Ag/Fe_3O_4@GO, some new peaks also appeared at 2θ of 32.2°, 40.1°, 46.1°, and 78.4°, corresponding to the 111, 200, 220, and 311 crystallographic planes of the face-centered

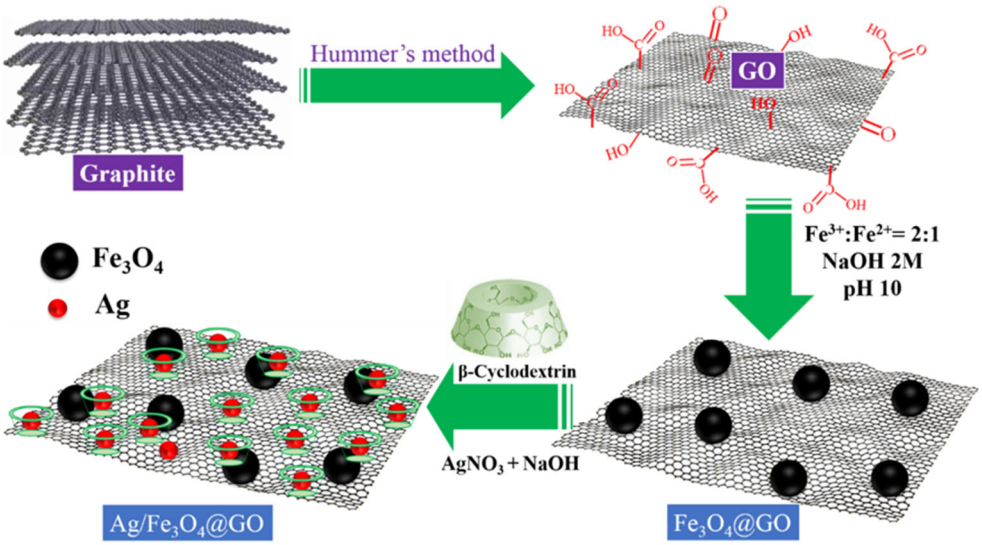

Scheme 1 Schematic illustration of the fabrication of Ag/Fe_3O_4@GO catalyst

cubic silver crystals, respectively (Kadam et al. 2018; Tran et al. 2020a). It should be noted that the diffraction peaks for GO were not observed after the decoration of Fe_3O_4 and AgNPs, which was probably due to the overlapping of high-intensity peaks of Fe_3O_4 and AgNPs (Kavyani and Baharfar 2020). This phenomenon was also observed in the study of Liu et al. (Liu et al. 2015).

Figure 1b shows the FTIR spectra of GO, Fe_3O_4@GO, and Ag/Fe_3O_4@GO. Obviously, the characteristic peaks of functional groups of GO were found in the FTIR spectra of all

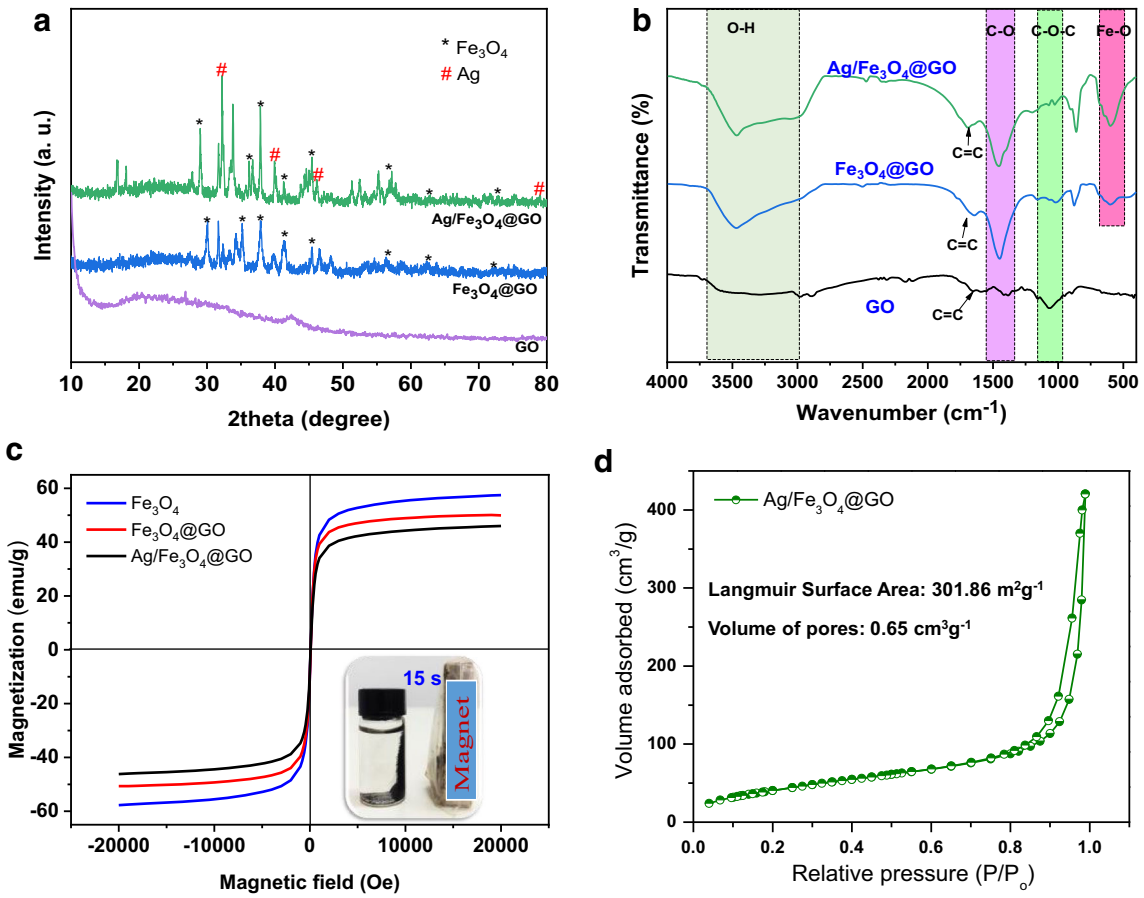

Fig. 1 XRD pattern (**a**) and FTIR spectra (**b**) of GO, Fe_3O_4@GO, and Ag/Fe_3O_4@GO samples; **c** magnetic hysteresis loops of Fe_3O_4, Fe_3O_4@GO, and Ag/Fe_3O_4@GO samples. The inset image is a photograph of Ag/Fe_3O_4@GO after separation with an external magnetic field; **d** nitrogen adsorption-desorption isotherm of Ag/Fe_3O_4@GO

three samples. Concretely, the broad band appeared at 3473 cm^{-1} was related to the stretching vibration of the O–H group (Tran et al. 2018). The absorbance peaks at 1287, 1424, and 1668 cm^{-1} were indexed to C–O–C, C–O, and C=C stretching vibrations, respectively. The aromatic C–H bending was observed at 860 cm^{-1}. The band at a wavelength of 582 cm^{-1} was assigned to the Fe–O vibrational band of Fe_3O_4 (Tran et al. 2020d). Regarding Ag/Fe_3O_4@GO, the characteristic band corresponding to the Fe–O bond was strong and red-shifted to a higher wavenumber of 612 cm^{-1} compared to that of 582 cm^{-1} of Fe_3O_4, suggesting that Fe_3O_4 was bound to the AgNPs (Li et al. 2013). These results proved the success of Ag/Fe_3O_4@GO synthesis.

Hysteresis loops of Fe_3O_4, Fe_3O_4@GO, and Ag/Fe_3O_4@GO composites are shown in Fig. 1c. All the samples incorporated with Fe_3O_4 NPs revealed a superparamagnetic behavior that was desirable for separation and reuse. Pure Fe_3O_4 exhibited a saturation magnetization at 57.6 emu/g. This value was slightly reduced to 50.1 emu/g when Fe_3O_4 NPs were wrapped with GO. In the case of Ag/Fe_3O_4@GO, the magnetization was further decreased to 45.7 emu/g. The decrease in the magnetization values was due to the increase of nonmagnetic materials (Ag, GO) (Li et al. 2013; Tran et al. 2020d). However, the magnetization level of Ag/Fe_3O_4@GO was still sufficient for the magnetic separation of nanocomposites from reaction mixtures, as displayed in the inset image of Fig. 1c**.** The Barrett-Joyner-Halenda (BJH) study of the isotherms of N_2 adsorption/desorption and distribution of pore size can be seen in Fig. 1d. The adsorption capacity, reflective of porosity, increases sharply at the end of the isothermal adsorption part (Tran and Lee 2018). With a pore volume of 0.65 cm^3/g, Ag/Fe_3O_4@GO has a Langmuir surface area of 301.86 m^2/g.

The FE-SEM images of Fe_3O_4, GO, Fe_3O_4@GO, and Ag/Fe_3O_4@GO and the TEM image of Ag/Fe_3O_4@GO are presented in Fig. 2. The SEM image of the Fe_3O_4 NPs represented the spherical morphology of Fe_3O_4 nanoparticles (Fig. 2a). Mostly, the NPs are in sphere form and agglomerated, which is due to the solution form of the sample. The particles have a narrow size distribution of about 12 nm. Figure 2b shows the FE-SEM image of GO flakes, revealing them to have a wavy, folded shape. SEM images of the GO indicated that it consisted of several layers stacked on top of one another like silky sheets of paper. Meanwhile, Fig. 2c shows different morphologies and structures of Fe_3O_4 spheres and GO layer, indicating that the Fe_3O_4 NPs were successfully decorated on the GO flakes. From Fig. 2d, it can be observed that more NPs were distributed on the surface of GO. The surface of Ag/Fe_3O_4@GO became more rough compared with bare GO, manifesting that Ag/Fe_3O_4 was well anchored and dispersed on the GO surface. The TEM image (Fig. 2e) clearly illustrated the distribution of Ag and Fe_3O_4 NPs on the surface of GO. It can be seen that the cubic crystals of Fe_3O_4 and Ag NPs were uniformly decorated on the transparent GO sheet with a high density and narrow size distribution of 10–20 nm.

The chemical composition of the Ag/Fe_3O_4@GO composites was verified by Energy dispersed X-ray spectrometer (EDX) spectra, as shown in Fig. 3a. The peaks for Ag/Fe_3O_4@GO

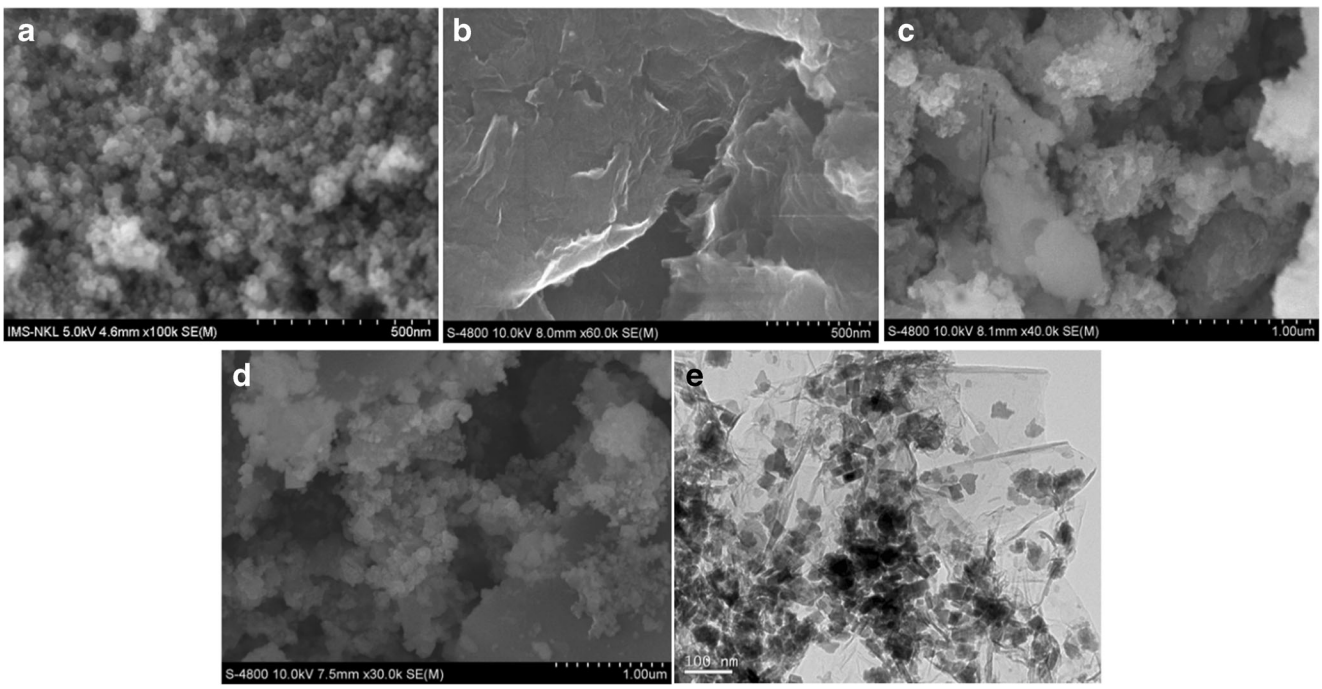

Fig. 2 FE-SEM images of Fe_3O_4 (**a**), GO (**b**), Fe_3O_4@GO (**c**), and Ag/Fe_3O_4@GO (**d**), and TEM image of Ag/Fe_3O_4@GO (**e**) sample

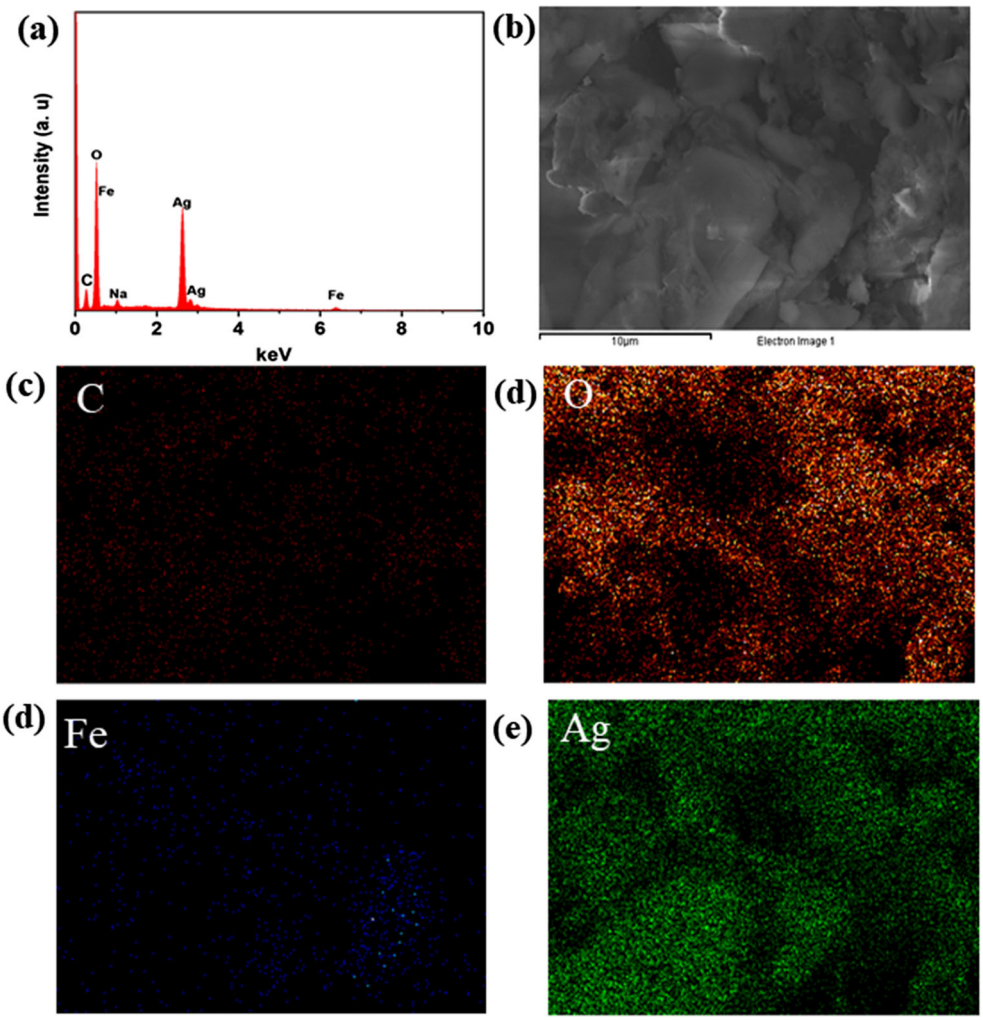

Fig. 3 **a** EDX spectrum of Ag/Fe_3O_4@GO; **b–f** correspond to the elemental mapping of composite Ag/Fe_3O_4@GO, C, O, Fe, and Ag, respectively.

composite were ascribed to Ag, Fe, C, and O elements. The small peak at 0.3 keV and the highest peak at 0.4 keV were associated with C and O elements, respectively. Significantly, the peaks at 2.7, 2.8, and 3.0 keV were contributed by the Ag element (Tran et al. 2020a). Besides, the EDX peaks at 0.35 and 6.4 keV identified the existent of the Fe element (Anh Tran et al. 2021). As can be noted that the Ag/Fe_3O_4@GO composite had reasonable purity, and all of the peaks were ascribed to the elements of the resultant composite. Besides, the distribution of these elements in the matrix of the nanocatalyst was mapped by a wavelength-dispersive X-ray spectroscope that was coupled to the FE-SEM instrument. The obtained elemental maps are displayed in Fig. 3b–f, which clarified the presence of well-dispersed Ag and Fe elements in the prepared nanocomposite. This figure also signified the presence of C and O that contributed by GO and β-CD (Veisi et al. 2019).

The catalytic activity of Ag/Fe_3O_4@GO

The catalytic activities of GO, Fe_3O_4@GO, and Ag/Fe_3O_4@GO were comparatively evaluated by measuring the reduction of MB and 4-NP with and without $NaBH_4$. The removal rates of MB and 4-NP over the different synthesized catalysts are presented in Fig. 4a and b, respectively. Obviously, the removal performance of both pollutants without the catalysts was low, reached about 10% (for MB) and 20% (for 4-NP) within 60 min. In the presence of the catalysts, the pollutant removal was greatly improved. The removal of MB and 4-NP by the GO + $NaBH_4$ and Fe_3O_4@GO + $NaBH_4$ systems occurred rapidly at the first 20 min and reached equilibrium at the efficiency of 45–50% for MB and 40–45% for 4-NP after 30 min of reaction time. Without $NaBH_4$, the Ag/Fe_3O_4@GO sample only removed 42% MB and 69% 4-NP after 60 min. Meanwhile, in the simultaneous existence of Ag/Fe_3O_4@GO and $NaBH_4$, the reduction of both MB and 4-NP significantly enhanced. About 36% of MB remained in the aqueous solution after 4 min, and this value continued to plummet to 18% after 6 min (Fig. 4a). The MB removal quickly reached 98% for 10 min, and MB was almost completely decomposed after 14 min. In the case of 4-NP reduction, Ag/Fe_3O_4@GO exhibited the same catalytic behavior as for MB, and the complete reduction was achieved after 16 min.

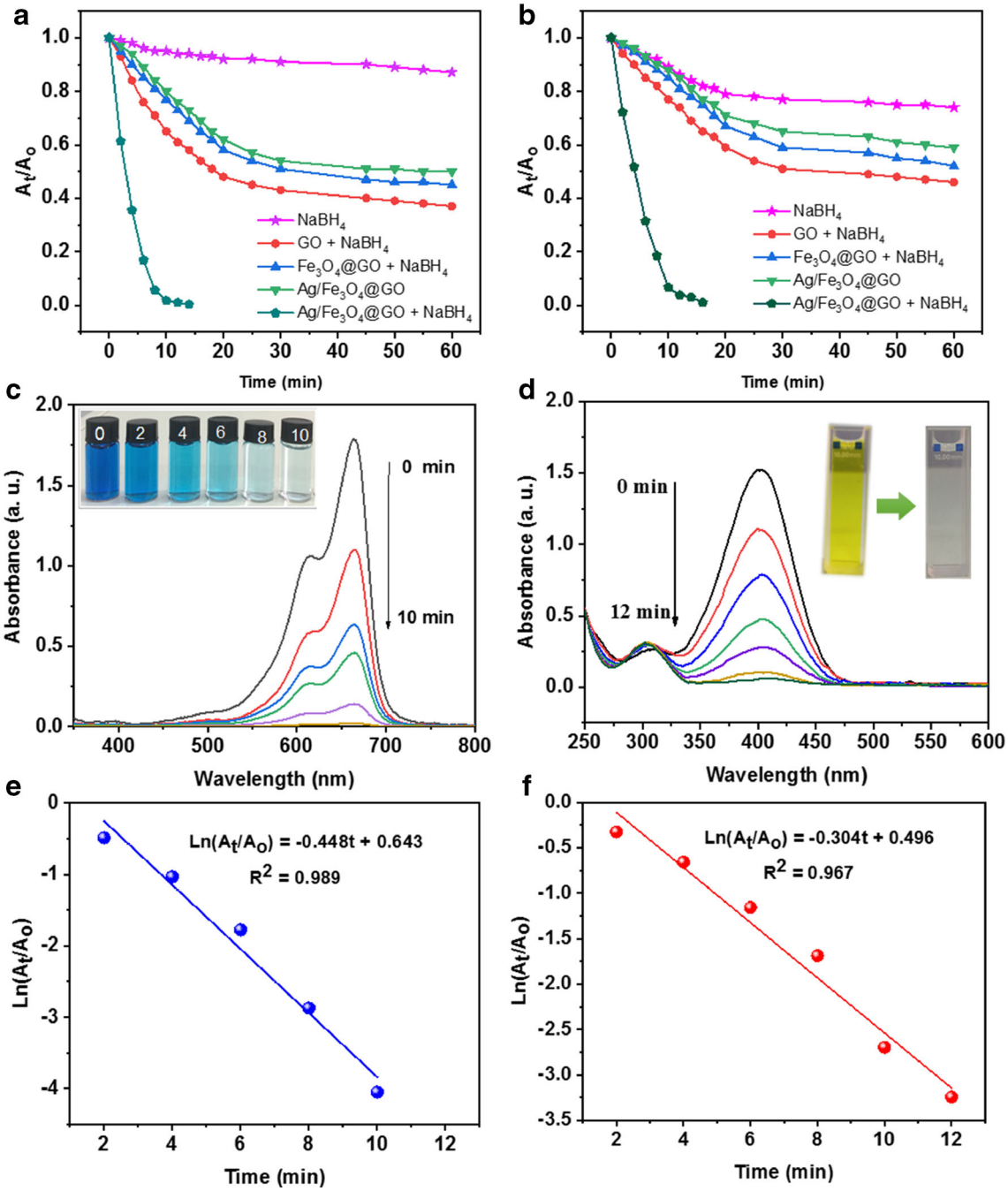

Fig. 4 Comparison of catalytic performances, time-dependent UV-Vis spectra, and linear fitting of $\ln(A_t/A_o)$ versus reaction time for MB (**a, c, e** and 4-NP **b, d, f** reduction

The reduction of MB and 4-NP by Ag/Fe_3O_4@GO in the presence of $NaBH_4$ was monitored using UV-Vis spectroscopy, as shown in Fig. 4 c and d. Thus, the catalytic activity of the prepared materials with the participation of $NaBH_4$ was shown in order of Ag/Fe_3O_4@GO > GO > Fe_3O_4@GO. The highest catalytic activity of Ag/Fe_3O_4@GO was contributed mainly by AgNPs embedded on the Fe_3O_4@GO surface (Tran et al. 2020a). The pristine GO exhibited higher catalytic performance than Fe_3O_4@GO, possibly due to its higher adsorption capacity (Tran et al. 2020b).

Since the concentration of $NaBH_4$ used in the catalytic process is much higher than that of MB and 4-NP, it is considered as a constant, and thus, the first-order kinetic equation ($\ln(A_t/A_o) = kt$) can be applied to determine the rate constant (k, min^{-1}) of the Ag/Fe_3O_4@GO composite (Doan et al. 2020). As shown in Fig. 4e and f, the plots of $\ln(A_t/A_o)$ versus reaction time had a linear relationship with high correlation

Table 1 Comparison of the nanocatalysts for the reduction of MB and 4-NP in the presence of $NaBH_4$

Pollutant	Catalyst	Catalyst dosage (mg/mL)	Concentration of pollutant (mM)	Rate constant (min^{-1})	References
MB	Fe_3O_4-EDTA-Ag	0.6	0.05	1.83	Sharif et al. (2019)
	Ag/Fe_3O_4@C	1.0	0.06	1.03	Zhu et al. (2013)
	Ag/rGO	0.003	0.16	0.014	Chengen et al. (2016)
	Fe_3O_4@C@Au	0.33	0.01	0.331	Gan et al. (2013)
	Fe_3O_4/rGO	0.003	0.005	0.050	Song et al. (2019)
	Ag/Fe_3O_4@GO	0.2	0.05	0.448	This study
4-NP	rGO/Fe_3O_4/Ag	0.0035	0.1	0.37	Xu et al. (2013)
	Au-Ag-γ-Fe_2O_3/rGO	0.01	0.1	0.013	Lei et al. (2018)
	Au/rGO/Ni	0.15	0.05	0.46	Cao et al. (2018)
	GO/Ag-Fe_3O_4	0.10	10.0	0.026	Qu et al. (2012)
	Au-GO	0.149	0.075	0.124	Choi et al. (2011)
	Ag/Fe_3O_4@GO	0.20	0.2	0.304	This study

coefficients (R^2 = 0.989 for MB and R^2 = 0.967 for 4-NP), indicating that the reduction of MB and 4-NP by Ag/Fe_3O_4@GO was well described the pseudo-first-order kinetics (Anh Tran et al. 2021). The apparent rate constants were found to be 0.448 and 0.304 min^{-1} for the MB and 4-NP, respectively. Compared with some other AgNPs-based catalyst (listed in Table 1), Ag/Fe_3O_4@GO exhibited relatively high catalytic activity, confirming its prospects for practical application.

Reusability study

To evaluate the stability of the catalyst, Ag/Fe_3O_4@GO was tested for the reduction of MB and 4-NP in the presence of $NaBH_4$ over five successive cycles. As shown in Fig. 5a, the Ag/Fe_3O_4@GO manifested a negligible decrease of catalytic activity for both MB and 4-NP even after five recycles. The slight decline of catalytic efficiency by ~2.64% is probably due to the loss of the catalyst during the recycling process. Notably, after five repeated use, the removal efficiency of Ag/Fe_3O_4@GO for MB and 4-NP still remained more than 97%, demonstrating high stability of the synthesized catalyst. XRD spectrum of Ag/Fe_3O_4@GO before and after reuse was investigated to evaluate its structural strength. As can be seen from Fig. 5b, there was no significant change in the positions and intensity of the diffraction peaks for the catalyst after using several times compared to the original. This result confirmed the high durability of Ag/Fe_3O_4@GO in the catalytic process. Moreover, the recoverability and leaching of the ternary Ag/Fe_3O_4@GO composite were also assessed. For these purposes, the recycled catalyst after the fifth run was recovered by magnetic separation, washed with distilled water several

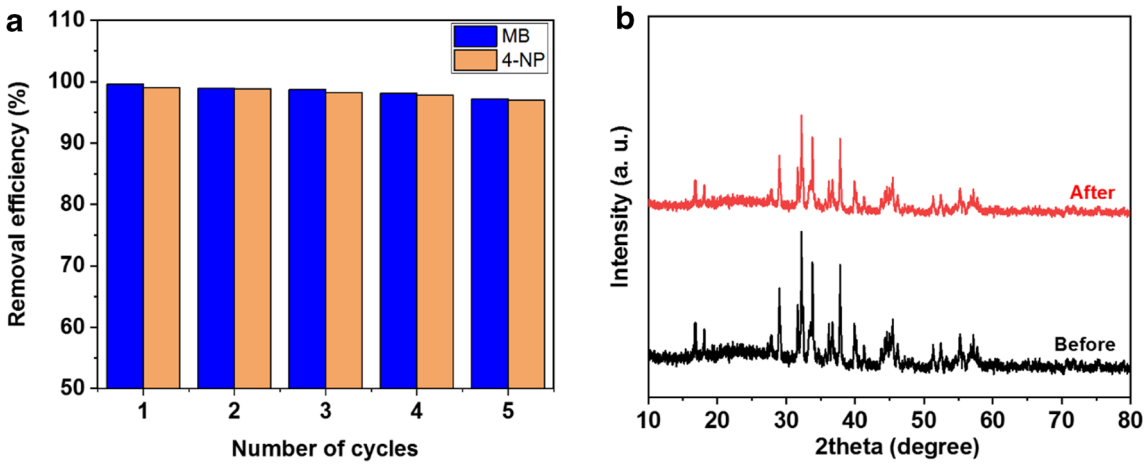

Fig. 5 **a** Reusability of Ag/Fe_3O_4@GO for the catalytic reduction of MB and 4-NP with the presence of $NaBH_4$; **b** XRD patterns of Ag/Fe_3O_4@GO before and after reuse

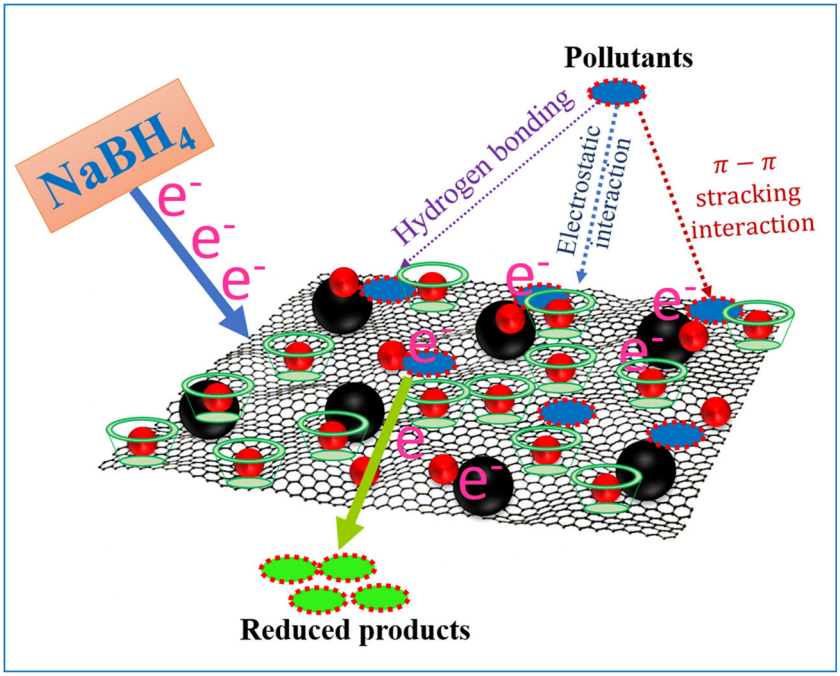

Scheme 2 Proposed reaction-mechanism for the catalytic reduction of MB and 4-NP by Ag/Fe_3O_4@GO supported by $NaBH_4$

times and dried to constant weight. Next, the ratio of the catalyst mass after use to its initial mass was calculated for evaluating the recoverability, while the concentration of silver and iron dissolved in the solution was tested by inductive coupled plasma mass spectrometry (ICP-MS) (Agilent 7700 series, USA) for analyzing the leaching of the material. The obtained results revealed that the material was well recovered using the magnetic separation with a high recoverability of 98.3%. At the same time, the leaching of the Ag/Fe_3O_4@GO composite was negligible, as evidenced by the low total dissolved silver (0.06 mg/L) and iron (0.27 mg/L) concentrations in the solution after five reuses. It is worth noting that the leaching of Ag and Fe ions was acceptable for wastewater according to the European Union discharge standards (< 0.1 mg/L for Ag and 2 mg/L for Fe) (Le et al. 2020). Thus, with high stability and strength, as well as good magnetic separation behavior, Ag/Fe_3O_4@GO can be reused long-term for catalytic reduction of organic pollutants.

Catalyst mechanism

The obtained results for MB and 4-NP reduction by different catalysts indicated that GO, Fe_3O_4@GO, Ag/Fe_3O_4@GO, or $NaBH_4$ have low catalytic effectiveness when used individually. The fast reduction of both MB and 4-NP was guaranteed by the simultaneous presence of Ag/Fe_3O_4@GO and $NaBH_4$. First, the MB and 4-NP molecules quickly adsorbed onto the surface of Ag/Fe_3O_4@GO via the following interaction forces: (i) the electrostatic attractions between negatively charged GO and positively charged adsorbates; (ii) π-π stacking interactions between the hexagonal skeleton of GO and the aromatic backbone of MB and 4-NP; and (iii) hydrogen-bonding interactions (Anh Tran et al. 2021b; Tran et al. 2020b). Next, the nucleophile (BH_4^-) in $NaBH_4$ enhanced the catalytic activity of Ag by donating the electrons to the AgNPs and activating them for the reaction with the pollutants. In this system, AgNPs acted as a relay that received an electron from $NaBH_4$ and transferred it to the pollutant molecules adsorbed in the Ag/Fe_3O_4@GO surface (Sharif et al. 2019). Furthermore, the large surface area and good electrical conductivity of GO ensured a fast mass and electron transport and facilitated the contact of pollutants with the catalyst surface. The main mechanistic pathways for the catalytic reduction of MB and 4-NP by Ag/Fe_3O_4@GO in the presence of $NaBH_4$ is illustrated in Scheme 2.

Conclusion

A highly efficient and stable ternary Ag/Fe_3O_4@GO catalyst for the reduction of organic pollutants in aqueous solution was successfully synthesized. β-CD appeared to be an excellent reducing and capping agent to decorate AgNPs on the GO sheet. The Ag/Fe_3O_4@GO nanocomposite/$NaBH_4$ system exhibited extraordinary reduction ability with an efficiency of over 98% for both MB and 4-NP after 10 min of reaction. The reduction kinetics followed a pseudo-first-order model with a rate constant of 0.448 min^{-1} and 0.304 min^{-1} for MB and 4-NP, respectively. The unusual catalytic activity of the developed material was supported by the strong synergistic effect of its multipurpose components (GO, Fe_3O_4, and AgNPs). The Ag/Fe_3O_4@GO catalyst showed high

recoverability of 98.3% due to the presence of superparamagnetic Fe_3O_4 NPs. Besides, the reusability study revealed that the designed composite possessed excellent stability (maintained over 97% after five repeated runs) and negligible leaching. Ultimately, the facile synthesis, high catalytic efficiency, and good reusability make the Ag/Fe_3O_4@GO nanocomposite a promising candidate for the application in catalytic reduction of organic pollutants from industrial wastewater.

Author contribution All authors contributed to the study conception and design. Material preparation, data collection, and analysis were performed by Van Dat Doan, Ngoc Vy Nguyen, and Thi Lan Huong Nguyen. The first draft of the manuscript was written by Van Thuan Le, and all authors commented on previous versions of the manuscript. Writing—review and editing was performed by Vy Anh Tran. All authors read and approved the final manuscript.

Funding This research is funded by Vietnam National Foundation for Science and Technology Development (NAFOSTED) under grant number 104.05-2019.03.

Data Availability All data generated or analyzed during this study are included in this published article.

Declarations

Ethics approval and consent to participate Not applicable

Consent for publication Not applicable

Competing interests The authors declare no competing interests.

References

Anh-Tran V, Vu KB, Vo TTT, Le VT, Do HH, Bach LG, Lee SW (2021) Experimental and computational investigation on interaction mechanism of Rhodamine B adsorption and photodegradation by zeolite imidazole frameworks-8. Appl Surf Sci 538:148065. https://doi.org/10.1016/j.apsusc.2020.148065

Cao M, Feng L, Yang P, Wang H, Liang X, Chen X (2018) Fabrication of reduced graphene oxide decorated with gold and nickel for the catalytic reduction of 4-nitrophenol. J Mater Sci 53:4874–4883. https://doi.org/10.1007/s10853-017-1913-9

Chengen HZL, Yun L, Leping H, Yingkui Y (2016) Graphene-supported silver nanoparticles with high activities toward chemical catalytic reduction of methylene blue and electrocatalytic oxidation of hydrazine. Int J Electrochem 11:9566–9574. https://doi.org/10.20964/2016.11.72

Choi Y, Bae HS, Seo E, Jang S, Park KH, Kim BS (2011) Hybrid gold nanoparticle-reduced graphene oxide nanosheets as active catalysts for highly efficient reduction of nitroarenes. J Mater Chem 21:15431–15436. https://doi.org/10.1039/C1JM12477C

Dao MU, Le HS, Hoang HY, Tran VA, Doan VD, Le TTN, Sirotkin A, Le VT (2020) Natural core-shell structure activated carbon beads derived from *Litsea glutinosa* seeds for removal of methylene blue: Facile preparation, characterization, and adsorption properties. Environ Res:110481. https://doi.org/10.1016/j.envres.2020.110481

Doan VD, Huynh BA, Nguyen TD, Cao XT, Nguyen VC, Nguyen TLH, Nguyen HT, Le VT (2020) Biosynthesis of silver and gold nanoparticles using aqueous extract of *Codonopsis pilosula* roots for antibacterial and catalytic applications. J Nanomater 2020:8492016–8492018. https://doi.org/10.1155/2020/8492016

Esmaeili N, Mohammadi P, Abbaszadeh M, Sheibani H (2019) Au nanoparticles decorated on magnetic nanocomposite (GO-Fe_3O_4/Dop/Au) as a recoverable catalyst for degradation of methylene blue and methyl orange in water. Int J Hydrog Energy 44:23002–23009. https://doi.org/10.1016/j.ijhydene.2019.07.025

Gan Z, Zhao A, Zhang M, Tao W, Guo H, Gao Q, Mao R, Liu E (2013) Controlled synthesis of Au-loaded Fe_3O_4@C composite microspheres with superior SERS detection and catalytic degradation abilities for organic dyes. Dalton Trans 42:8597–8605. https://doi.org/10.1039/C3DT50341K

Ismail M, Akhtar K, Khan MI, Kamal T, Khan MA, A MA, Seo J, Khan SB (2019) Pollution, toxicity and carcinogenicity of organic dyes and their catalytic bio-remediation. Curr Pharm Des 25:3645–3663. https://doi.org/10.2174/1381612825666191021142026

Kadam AN, Bhopate DP, Kondalkar VV, Majhi SM, Bathula CD, Tran AV, Lee SW (2018) Facile synthesis of Ag-ZnO core–shell nanostructures with enhanced photocatalytic activity. J Ind Eng Chem 61:78–86. https://doi.org/10.1016/j.jiec.2017.12.003

Kavyani S, Baharfar R (2020) Design and characterization of Fe_3O_4/GO/Au-Ag nanocomposite as an efficient catalyst for the green synthesis of spirooxindole-dihydropyridines. Appl Organomet Chem 34:e5560. https://doi.org/10.1002/aoc.5560

Kumari S, Sharma P, Yadav S, Kumar J, Vij A, Rawat P, Kumar S, Sinha C, Bhattacharya J, Srivastava CM, Majumder S (2020) A novel synthesis of the graphene oxide-silver (GO-Ag) nanocomposite for unique physiochemical applications. ACS Omega 5:5041–5047. https://doi.org/10.1021/acsomega.9b03976

Le TTN, Le VT, Dao MU, Nguyen QV, Vu TT, Nguyen MH, Tran DL, Le HS (2019) Preparation of magnetic graphene oxide/chitosan composite beads for effective removal of heavy metals and dyes from aqueous solutions. Chem Eng Commun 206:1337–1352. https://doi.org/10.1080/00986445.2018.1558215

Le VT, Doan VD, Tran VA, Le HS, Tran DL, Pham TM, Tran TH, Nguyen HT (2020) Cu/Fe_3O_4@carboxylate-rich carbon composite: one-pot synthesis, characterization, adsorption and photo-Fenton catalytic activities. Mater Res Bull 129:110913. https://doi.org/10.1016/j.materresbull.2020.110913

Lei G, Ma J, Li Z (2018) Magnetic Au-Ag-γ-Fe_2O_3/rGO Nanocomposites as an efficient catalyst for the Reduction of 4-Nitrophenol 8(11):877. https://doi.org/10.3390/nano8110877

Li N, Huang GW, Shen XJ, Xiao HM, Fu SY (2013) Controllable fabrication and magnetic-field assisted alignment of Fe_3O_4-coated Ag nanowires via a facile co-precipitation method. J Mater Chem C 1:4879–4884. https://doi.org/10.1039/C3TC30270A

Lim EB, Tran AV, Lee SW (2020) Comparative release kinetics of small drugs (ibuprofen and acetaminophen) from multifunctional mesoporous silica nanoparticles. J Mater Chem B 8:2096–2106. https://doi.org/10.1039/C9TB02494H

Liu G, Jiang W, Wang Y, Zhong S, Sun D, Liu J, Li F (2015) One-pot synthesis of Ag@Fe_3O_4/reduced graphene oxide composite with excellent electromagnetic absorption properties. Ceram Int 41:4982–4988. https://doi.org/10.1016/j.ceramint.2014.12.063

Liu YY, Zhao YH, Zhou Y, Guo XL, Chen ZT, Zhang WJ, Zhang Y, Chen J, Wang ZM, Sun LT, Zhang T (2018) High-efficient catalytic reduction of 4-nitrophenol based on reusable Ag nanoparticles/graphene-loading loofah sponge hybrid. Nanotechnology 29:315702. https://doi.org/10.1088/1361-6528/aac3e8

Luu TVH, Luu MD, Dao NN, Le VT, Nguyen HT, Doan VD (2020) Immobilization of C/Ce-codoped ZnO nanoparticles on multi-walled carbon nanotubes for enhancing their photocatalytic activity.

J Dispers Sci Technol:1-12. https://doi.org/10.1080/01932691.2020.1740728

Ma YP, Mu BL, Zhang XJ, Xu HM, Qu Z, Gao L, Li B, Tian JJ (2019) Ag-Fe_3O_4@rGO ternary magnetic adsorbent for gaseous elemental mercury removal from coal-fired flue gas. Fuel 239:579–586. https://doi.org/10.1016/j.fuel.2018.11.065

Mao H, Ji C, Liu M, Cao Z, Sun D, Xing Z, Chen X, Zhang Y, Song X-M (2018) Enhanced catalytic activity of Ag nanoparticles supported on polyacrylamide/polypyrrole/graphene oxide nanosheets for the reduction of 4-nitrophenol. Appl Surf Sci 434:522–533. https://doi.org/10.1016/j.apsusc.2017.10.209

Nariya P, Das M, Shukla F, Thakore S (2020) Synthesis of magnetic silver cyclodextrin nanocomposite as catalyst for reduction of nitro aromatics and organic dyes. J Mol Liq 300:112279. https://doi.org/10.1016/j.molliq.2019.112279

Nguyen V-H, Thi Vo T-T, Huu Do H, Thuan Le V, Duy Nguyen T, Ky Vo T, Nguyen B-S, Tai Nguyen T, Khoa Phung T, Anh Tran V (2020) Ag@ZnO porous nanoparticle wrapped by rGO for the effective CO_2 electrochemical reduction. Chem Eng Sci:116381. https://doi.org/10.1016/j.ces.2020.116381

Qu JC, Ren CL, Dong YL, Chang YP, Zhou M, Chen XG (2012) Facile synthesis of multifunctional graphene oxide/AgNPs-Fe_3O_4 nanocomposite: A highly integrated catalysts. Chem Eng J 211-212:412–420. https://doi.org/10.1016/j.cej.2012.09.096

Sharif HMA, Mahmood A, Cheng HY, Djellabi R, Ali J, Jiang WL, Wang SS, Haider MR, Mahmood N, Wang A-J (2019) Fe_3O_4 nanoparticles coated with EDTA and Ag nanoparticles for the catalytic reduction of organic dyes from wastewater. ACS Applied Nano Mater 2:5310–5319. https://doi.org/10.1021/acsanm.9b01250

Song S, Wang Y, Shen H, Zhang J, Mo H, Xie J, Zhou N, Shen J (2019) Ultrasmall graphene oxide modified with Fe_3O_4 nanoparticles as a fenton-like agent for methylene blue degradation. ACS Applied Nano Mater 2:7074–7084. https://doi.org/10.1021/acsanm.9b01608

Tran VA, Lee SW (2018) A prominent anchoring effect on the kinetic control of drug release from mesoporous silica nanoparticles (MSNs). J Colloid Interface Sci 510:345–356. https://doi.org/10.1016/j.jcis.2017.09.072

Tran AV, Shim K, Vo TTT, Kook JK, An SSA, Lee SW (2018) Targeted and controlled drug delivery by multifunctional mesoporous silica nanoparticles with internal fluorescent conjugates and external polydopamine and graphene oxide layers. Acta Biomater 74:397–413. https://doi.org/10.1016/j.actbio.2018.05.022

Tran VA, Kadam AN, Lee SW (2020a) Adsorption-assisted photocatalytic degradation of methyl orange dye by zeolite-imidazole-framework-derived nanoparticles. J Alloys Compd 835:155414. https://doi.org/10.1016/j.jallcom.2020.155414

Tran VA, Nguyen TP, Le VT, Kim I-T, Lee SW, Nguyen TC (2020b) Excellent photocatalytic activity of ternary Ag@WO_3@rGO nanocomposites under solar simulation irradiation. J Sci Adv Mater Dev 6:108–117. https://doi.org/10.1016/j.jsamd.2020.12.001

Tran VA, Shim K, Lee SW, An SSA (2020c) Multimodal mesoporous silica nanocarriers for dual stimuli-responsive drug release and excellent photothermal ablation of cancer cells. Int J Nanomedicine 15:7667–7685. https://doi.org/10.2147/IJN.S254344

Tran VA, Tran NHT, Bach LG, Nguyen TD, Nguyen TT, Nguyen TT, Nguyen TAN, Vo TK, Vo TTT, Le VT (2020d) Facile synthesis of propranolol and novel derivatives. J Chem 2020:9597426–9597410. https://doi.org/10.1155/2020/9597426

Tran AV, Khoa PT, Thuan LV, Ky VT, Tai NT, Anh Nga NT, Quoc VD, Quang HV, Vo TTT (2021) Solar-light-driven photocatalytic degradation of methyl orange dye over Co_3O_4-ZnO nanoparticles. Mater Lett 284:128902. https://doi.org/10.1016/j.matlet.2020.128902

Veisi H, Razeghi S, Mohammadi P, Hemmati S (2019) Silver nanoparticles decorated on thiol-modified magnetite nanoparticles (Fe_3O_4/SiO_2-Pr-S-Ag) as a recyclable nanocatalyst for degradation of organic dyes. Mater Sci Eng C 97:624–631. https://doi.org/10.1016/j.msec.2018.12.076

Xu S, Yong L, Wu P (2013) One-Pot, Green, Rapid synthesis of flower-like gold nanoparticles/reduced graphene oxide composite with regenerated silk fibroin as efficient oxygen reduction electrocatalysts. ACS Appl Mater Interfaces 5:654–662. https://doi.org/10.1021/am302076x

Xu Y, Shi X, Hua R, Zhang R, Yao Y, Zhao B, Liu T, Zheng J, Lu G (2020) Remarkably catalytic activity in reduction of 4-nitrophenol and methylene blue by Fe_3O_4@COF supported noble metal nanoparticles. Appl Catal B Environ 260:118142. https://doi.org/10.1016/j.apcatb.2019.118142

Yazdani F, Seddigh M (2016) Magnetite nanoparticles synthesized by co-precipitation method: The effects of various iron anions on specifications. Mater Chem Phys 184:318–323. https://doi.org/10.1016/j.matchemphys.2016.09.058

Zhu M, Wang C, Meng D, Diao G (2013) In situ synthesis of silver nanostructures on magnetic Fe_3O_4@C core–shell nanocomposites and their application in catalytic reduction reactions. J Mater Chem A 1:2118–2125. https://doi.org/10.1039/C2TA00669C